Comparative study of catalytic activity of Pd loaded hydroxyapatite and fluoroapatite in butan-2-ol conversion and methane oxidation

Zouhair Boukha [a,b], Mohamed Kacimi [a], Mahfoud Ziyad [a,*], Alain Ensuque [b], François Bozon-Verduraz [b]

[a] *Faculté des Sciences, Laboratoire de Physico-chimie des Matériaux et Catalyse, Département de Chimie, Avenue Ibn Battouta, B.P. 1014, Rabat, Morocco*

[b] *ITODYS, UMR-CNRS 7086, Université Denis Diderot, Paris 7, 2 place Jussieu, Paris, France*

* Corresponding author. ziyad@fsr.ac.ma

Tel.: +212 37 77 56 34

Fax: +212 37 77 56 34.

Abstract

Palladium loaded calcium-hydroxyapatite, Pd(*z*)/CaHAp, and calcium-fluoroapatite, Pd(*z*)/CaFAp, were synthesised and characterised by TEM, XRD, IR and UV–vis–NIR spectroscopies. Introduction of palladium does not change the structure of CaHAp and CaFAp. The average size of PdO particles was found to be around 4–5 nm on Pd(1)/CaHAp but larger (6–7 nm) on Pd(1)/CaFap. The acid–base properties of the supports and of the catalysts were studied using butan-2-ol conversion. On CaHAp and CaFAp, the butenes yield (dehydration reaction) is very low either in the absence or in the presence of oxygen. The methyl ethyl ketone yield (dehydrogenation reaction) is significant only in the presence of oxygen and higher over CaFAp. Conversely, the performances of Pd(*z*)/CaHAp are better than those of Pd(*z*)/CaFAp below 180 °C. Above 180 °C, buta-2-ol combustion is favoured on Pd/CaHAp but not on Pd/CaFAp.

In methane oxidation, Pd(*z*)/CaHAp showed also a much larger activity than Pd(*z*)/CaFAp. On 2 wt% Pd loaded CaHAp, the methane oxidation reaches a conversion of almost 100% at 350 °C, which is comparable with the performance of conventional Pd/Al_2O_3 catalysts. The reducibility of PdO under methane–oxygen mixtures is lower on Pd(*z*)/CaHAp. For both reactions, the lower activity of Pd(*z*)/CaFAp is related to its higher acidity, resulting from the substitution of OH^- by F^-, and to the larger PdO particle size.

Keywords: Calcium-hydroxyapatite; Calcium-fluoroapatite; Palladium and palladium oxide; Methane combustion; Butan-2-ol conversion; TEM; UV–vis–NIR; IR spectroscopy

1. Introduction

The proven reserves of methane are quite significant. This combustible represents today, with the decay of oil supplies, an important alternative for the replacement and the diversification of the conventional sources of energy. It has an important calorific power and it is already largely employed in industrial heat generators. However, its direct lighting requires high temperatures and generates damaging pollutants for the environment.

The catalytic combustion of CH_4 has attracted much atten- tion in the last years. The investigations were essentially focused on the preparation of active and stable catalysts [1–9]. Current research is dedicated to the synthesis of supports less sensitive to sintering and exhibiting suitable acid–base properties.

According to many authors, the oxidation state of palladium plays a decisive role in its activity [10]. Several authors claimed that the active sites are constituted by PdO. Others have estab- lished that the activity is due to the interaction between Pd and PdO when the catalyst is working. In their study of the PdO_x/ZrO_2 system, Fujimoto et al. reported that the methane combustion at low temperature is favoured by the presence of oxygen atoms and oxygen vacancies on the catalyst sur- face [11]. Carstens et al. noticed an agglomeration of PdO crystallites in the presence of methane and PdO surface restructuration in pure oxygen [12]. Recently, Lin et al. studied the $PdO/ZrO_2–TiO_2$ system and showed that the best catalytic performance is achieved when the catalyst contains both Pd and PdO [13]. It has been claimed that CH_4 oxidation involves complex reaction pathways inducing a switching back and forth between the surface predominance of either Pd or PdO [14]. These redox processes provoke strong superficial changes and are generally accompanied by an oscillatory behaviour of the catalytic activity. As a matter of fact, hystereses activity have been observed on different catalysts submitted, in continuous reactor, to cycles of temperature and reaction mixtures containing oxygen [15,16].

In addition, the nature of the support and the palladium particle size play an important role in the

catalytic behaviour of these systems [17–19]. The rate of palladium oxidation is believed to be influenced by the Pd particles size, the small particles showing a higher tendency to be oxidized [20]. Many catalysts, including those industrially used in hydrotreatment reactions, contain phosphorus in the form of phosphates. The $(PO_4)^{3-}$ groups stabilize the structure of active centres and allow the adjustment of the acid-base properties [21].

The general formula of stoichiometric apatites is $M_{10}(XO_4)_6Y_2$ [22]. Fluoroapatite Ca10(PO4)6F2 is struc- turally isomorphous to this family of compounds which constitutes the major component of the natural rock phosphates. It crystallizes in the hexagonal system and belongs to $P6_3/m$ (C_{6h}) space group. The framework of the apatitic structures consists of a quasi compact ensemble of tetrahedral $(PO_4)^{3-}$ ions which delimit two types of zeolite-like channels. The first type has an average diameter of 2.5 Å and is bordered by the Ca^{2+} cations noted Ca(I). The second type has an average diameter of 3.5 Å and it plays an essential role in the properties of apatites. It can host ions such as OH^-, Cl^-, Br^-, F^- or oxygen species under special conditions [16]. Furthermore, the structure of apatites allows different substitutions and ion exchanges. The Ca^{2+} ions can be partially replaced by bivalent cations (Pb^{2+}, Sr^{2+}, Zn^{2+}, Fe^{2+}, Cu^{2+}, Ba^{2+}, . . .) and perhaps also by trivalent species. The $(PO_4)^{3-}$ groups can be substituted by anions such as arsenates, vanadates, chromates. This structural flexibility confers to the apatites their various properties [23–25].

Despite their numerous applications, apatites have called limited attention in the field of heterogeneous catalysis. This family of phosphates is known to exhibit basic properties, which can be modulated by different cation exchanges [24–26]. Hall have shown that the stoichiometric hydroxyapatite is active in the dehydrogenation as well as in the dehydra- tion of butan-2-ol whereas the non-stoichiometric apatite (Ca/P = 1.58) leads only to the dehydration reaction [26]. The dehydration activity increases with the catalyst acidity and the calcium deficiency. Concomitantly, the dehydrogenation activ- ity decreases with the basic character of the solid [23–27]. The exchange of Ca^{2+} ions with Cu^{2+} or Ni^{2+} confers to the phosphate dehydrogenating

ability and redox properties [27].

The present work concerns the study of the behaviour of palladium loaded hydroxyapatite and fluoroapatite in methane oxidation reaction. Special attention will be devoted to the acid–base properties of the carrier and to their influence on the efficiency of palladium in the reaction. The substitution of OH^- by F^- changes the acid–base features of apatite and probably also its interaction with Pd. Several samples of hydroxyapatite and fluoroapatite were synthesized and their acid-base proper- ties were characterized using butan-2-ol conversion as probe reaction. The catalysts were also characterized by MET, XRD, IR and UV–vis spectroscopies in order to correlate their activity to the structural features.

2. Experimental

2.1. Catalysts

Several methods have been used for the synthesis of pure apatites. The simplest one is the neutralisation of a calcium hydroxide solution $Ca(OH)_2$ by phosphoric acid and the most employed is the double decomposition method which consists of mixing, drop wise, an ammonical solution of calcium nitrate with a solution of $(NH_4)_2HPO_4$ [28–30].

In the present study, calcium-hydroxyapatite (CaHAp) and calcium-fluoroapatite (CaFAp) were prepared using a modified version of the two previous methods. A boiled solution of calcium nitrate (1 M) was added drop wise to a solution of $(NH_4)_2HPO_4$ (0.6 M) (which in the case of CaFAp contains also an excess of NH_4F). The obtained precipitate was redissolved by adding a 2 M nitric acid solution. The resulting mixture was neutralised with ammonia to pH 9, then maintained under stirring at 80 °C for 24 h. The recovered product was washed and filtered with boiling purified water before drying at 120 °C and calcination during 12 h at 550 °C in air.

Palladium loaded CaHAp and CaFAp were prepared by the impregnation method using solutions containing different amounts of $Pd(NO_3)_2(NH_3)_4$. The apatite was dispersed in the

palladium solution (pH # 8) and kept boiling at reflux for 1 h before heating to dryness. The recovered solid was calcined during 12 h at 550 °C in air. The samples were labelled Pd(z)/CaHAp for the loaded calcium-hydroxyapatite and Pd(z)/CaFAp for the calcium-fluoroapatite, respectively. The loaded amount of palladium is represented by (z) and it corresponds to the real Pd weight percentage in the catalyst, determined by chemical analyses ($0.3 \leq z \leq 2.0$ wt%).

2.2. Characterisation techniques

The specific surfaces areas were measured using nitrogen adsorption at −196 °C with a Micromeritics apparatus. The results are reported in Table 1. CaHAp has a higher surface area than CaFAp. The Pd impregnation process does not seem to notably modify surface areas of the samples.

Chemical analyses were performed (at CNRS-Vernaison) using an inductive coupling plasma–atomic spectroscopy (ICP–AES). The results are also summarized in Table 1.

Transmission electron microscopy (TEM) observations were carried out with a Joel CXII microscope operating at 100 kV. The sample powder was dispersed in ethanol, one drop of the suspension was deposited on the carbon membrane of the microscope grid and the solvent was evaporated at room temperature.

X-ray powder diffraction patterns were obtained with a Siemens D5000 apparatus equipped with a cobalt anticathode (Kα = 1.78). The data were collected at room temperature with a step size of 0.02 degree/s in 2θ, from $2\theta = 15^{\circ}$ to 60°. The crystalline phases were identified by comparison with ICSD reference files [31].

FTIR transmission spectra were recorded in the 400–4000 cm^{-1} range with a Bruker Equinox spectrometer using disks of samples diluted in KBr. This technique was principally employed to verify the absence of the band at 875 cm^{-1} usually attributed to $(HPO_4)^{2-}$ ions that might give rise to pyrophosphates.

Diffuse reflectance spectra were recorded at room temperature between 190 and 2500 nm on a Varian Cary 5E spectrometer equipped with a double monochromator and an integrating sphere coated with polytetrafluoroethylene (PTFE). PTFE was used at the same time as a reference.

2.3. Catalytic tests

Catalytic conversion of butan-2-ol was studied in a continuous-flow reactor at atmospheric pressure in order to char- acterize the acid–base properties of the catalysts. The typical run was performed between 120 and 260 °C, on 100 mg of catalyst sieved to 120–180 μm and maintained in the reactor between quartz wool plugs. Butan-2-ol was supplied to the reactor diluted in N_2 or air at a partial pressure equal to 840 Pa and a total flow rate of 60 cm^3 min^{-1}.

The catalytic activity of the sample was also measured in CH_4 oxidation using a quartz continuous flow microreactor operated at atmospheric pressure. Prior to the reaction 100 mg of the catalyst were sieved to a grain size ranging from 120–180 μm, and placed into the reactor between two quartz wool plugs. The reaction mixture was composed of 1 vol% CH_4 and 99 vol% of air in a total flow rate of 100 cm^3 min^{-1}. The temperature of reaction was increased from room temperature up to 900 °C with a heating rate of 5 °C mn^{-1}. Analyses of the effluent gases were performed using two online chromatographs; one FID for hydro- carbons separation on a 2 m Porapak Q column and another one equipped with catharometers and a silica gel column for the oxygenated products.

3. Results and discussion

3.1. Catalysts characterization

3.1.1. Transmission electron microscopy (TEM)

Pd loaded and unloaded phosphates were investigated by transmission electron microscopy. The micrographs of CaHAP and CaFAP calcined at 550 °C show no difference in morphology. In both cases the particles have a quasi-spherical shape (not shown).

Figs. 1 and 2 show the TEM micrographs and size distribution diagrams (determined from 200 pictures) of Pd(1)/CaHAp and Pd(1)/CaFAp. Examination of Pd(1)/CaHAp (Fig. 1a) reveals the presence of small PdO particles (mean particle size is 4.4 nm), whereas on Pd(1)/CaFAp (Fig. 2b), the mean particle size is larger (6–7 nm).

3.1.2. XRD patterns

X-ray diffraction patterns of CaHAp and CaFAp (not shown) are similar confirming that both solids are monophasic and have apatitic structure. All the peaks were indexed in the hexagonal system with the space group $P6_3/m$ (ICSD, n°16742). The addition of palladium to the apatites and the successive treatments at 550 °C do not modify the structure of the supports and no peak due to PdO or Pd is observed probably because the Pd amount and/or the size of diffracting domains is too small as confirmed by TEM observations.

3.1.3. IR spectra

The recorded FTIR spectra are characteristic of the apatites (Fig. 3). They are composed of three different domains. The first one extends from 400 to 1200 cm^{-1}. It contains the vibration modes of P-O bonds of $(PO_4)^{3-}$ groups which are characterized by three bands that appear at 965, 1035 and 1094 cm^{-1} [28–30]. The small and sharp band at 3566 cm^{-1} is due to the vibration modes of the O-H groups hosted by the apatite framework. It might also be noted that there is no band around 875 cm^{-1}, which attests the absence of $(HPO_4)^{2-}$. These species lead to pyrophosphates after calcination above 600 °C.

The region extending from 1300 to 1600 cm^{-1} contains two bands centred on 1395 and 1457 cm^{-1}. They are attributed to carbonate species that appear in the samples exposed to CO_2. The bands located at 1626 and 3400 cm^{-1} are associated with the bending and stretching vibrations of water molecules. In 3775–3530 cm^{-1} and 750–620 cm^{-1} ranges, calcium-hydroxyapatite shows bands attributed to the symmet ric stretching (ν_s) and the bending vibration of hydroxyl groups (ν_L) [30]. These bands are, as expected, absent from the spectrum of fluoroapatite.

The addition of palladium to CaHAp and CaFAp does not modify the IR spectra as previously observed for X-ray diffrac- tion patterns.

3.1.4. UV–vis-NIR DRS

The UV–vis spectra of Pd(*z*)/CaHAp catalysts are pre- sented in Fig. 4. The spectrum of pure CaHAp (Fig. 4a) exhibits several bands due to ν_{OH} overtones of surface hydroxyl groups (1385 and 1425 nm) and a combination of ν_{OH} and δ_{OH} (1850–2300 nm). In the UV region, there is only a maximum around 200 nm ascribed to $O^{2-} \rightarrow Ca^{2+}$ charge transfers. After loading CaHAp with different amounts of palladium, new bands appear in UV–vis region (Fig. 4): (i) a band at 250 nm assigned to a $O^{2-} \rightarrow Pd^{2+}$ charge transfers; (ii) a broad band centred on 415 nm which tends to split in two bands centred on 375 and 475 nm for palladium percentages ≥0.5 wt%.

Conversely to Pd(*z*)/CaHAp, Pd(*z*)/CaFAp (Fig. 5) does not display the band at 1425 nm, which indicates the substitution of OH groups by fluorine (see also the IR spectra of Fig. 3). In the UV–vis region, the spectrum (Fig. 5) shows also absorption massif between 200 and 600 nm, constituted by overlapping bands centred near 250 nm, 375 and 475 nm (with a shoulder near 275 nm at higher Pd contents).

The attribution of these bands was carried out by comparison with spectra of reference compounds prepared at different temperatures and under various redox atmospheres. Rakai et al. showed that the tetrachloropalladate ion $(PdCl_4)^{2-}$ exhibits four bands among which three appear at 280, 340 and 475 nm [32]. They were assigned to charge transfers and d–d transitions of Pd^{2+} ions in D_{4h} symmetry. After a treatment in O_2 above 250 °C, the complex loses chlorine and gives rise to three bands centred on 255, 340 and 450 nm. When the reference compound is a palladium acetylacetonate decomposed above 200 °C in O_2, only two bands located at 255 and 450–460 nm remain in the spectrum [32], which can be ascribed to d–d transition of tetra-coordinated Pd^{2+} in oxygen environment. Table 2 lists these bands and their attribution for different reference compounds and carriers.

However, the presence of a marked absorption edge below 750 nm (Figs. 4 and 5) suggested that

the majority of Pd^{2+} ions form PdO ensembles or clusters. Bulk PdO, indeed, is a p type semiconductor with a narrow band gap (0.7 eV). Its absorption edge appears around 1700 nm, but for nanosized particles (< 20 nm), this edge shifts toward the visible domain because of the quantum size effect [32,33]. For Pd(*z*)/CaHAp catalysts series, this absorption edge calculated according to a procedure previously described by Weber [34], is shifted down to 2.2 eV (560 nm) (Fig. 4), which explains the pink colour of the samples instead of the brown one of large PdO particles. For Pd(*z*)/CaFAp, the edge position can be estimated to about 750 nm (1.7 eV). These results are in agreement with the data of TEM analysis.

3.2. Catalytic tests

3.2.1. Butan-2-ol conversion

The catalytic activity of butan-2-ol conversion was used to characterise the acid–base properties of CaHAp, CaFAp, Pd(*z*)/CaHAp and Pd(*z*)/CaFAp (Figs. 6–9). This reaction allows also the characterisation of the catalysts redox properties by investigating their oxidative dehydrogenation abilities [35,36]. On CaHAp and CaFAp, the butenes yield (dehydration reac- tion) is very low, either in the absence or in the presence of oxygen (Figs. 6 and 8, respectively). For example, at 260 °C in N_2 (Fig. 6), the butenes yield reaches only 1.5% on CaHAp and around 3% on CaFAp, although the specific surface area of CaHAp is higher (Table 1). This small difference in conversion suggests that the surface of CaFAp bears more Brönsted acid sites than that of CaHAp, in agreement with previous work on fluorinated alumina [36].

Addition of palladium to the carriers modifies completely their behaviour. The butenes yield (Fig. 6) is now greater over Pd(1)/CaHAp than over Pd(1)/CaFAp either in N_2 (Fig. 6) or in air (Fig. 8) but remains very low in both cases. This inversion of activity may be ascribed to the changes of the surface acidity induced probably by the impregnation process [30].

The dehydrogenation (methyl ethyl ketone MEK production) predominates over dehydration (butenes formation) on the sup- ports and catalysts (Figs. 7 and 9). On CaHAp and CaFAp, at 260

˚C in the absence of O_2 (Fig. 7), it reaches 5% on CaHAp and 10% on CaFAp. Usually, the dehydrogenation reaction in absence of O_2 takes place on basic sites such as Ca^{2+}–O^{2-} pairs, which can abstract hydrogen atoms from the alcohol [37]. The greater activity of fluoroapatite suggests that CaFAp possesses, in agreement with electronegative properties of F^-, more efficient Lewis basic sites than CaHAp. In the presence of O_2 (Fig. 9), there is a marked increase of MEK yield, with a greater activity for CaFAp. This activity was attributed to the basic properties of F^- ions.

On Pd(1)/CaHAp and Pd(1)/CaFAp, the methyl ethyl ketone (MEK) yield is much higher but the activity order is reversed (Fig. 9). On Pd(1)/CaHAp, the reaction starts around 60 ˚C and reaches a maximum (90%) at 170 ˚C before decreasing sharply for $T \geq 180$ ˚C with a high CO_2 production. On Pd(1)/CaFAp, the reaction starts near 130 ˚C and the MEK yields increase continuously (50% at 180 ˚C, 87% at 260 ˚C) without any production of CO_2. The high activity of Pd(1)/CaHAp in butan-2-ol combustion might be exploited in the catalytic combustion of volatile organic compounds, strongly involved in environmental protection. It can probably be explained by the ability of this catalyst to adsorb O_2 and produce oxygen species, favouring the dehydrogenation reaction and the combustion of the MEK formed [38].

3.2.2. Methane combustion

Figs. 10 and 11 display the CH4 conversion data over Pd(z)/CaHAp and Pd(z)/CaFAp in the form of light-off curves versus temperature for different Pd loadings. Without catalyst, the reaction starts above 700 ◦C. With the reactor filled up with pure CaHAp or CaFAp the reaction begins around 500 ˚C and 700 ˚C, respectively. At 550 ˚C, the methane conversion is close to 10% on CaHAp and is negligible on CaFAp.

Addition of Pd to CaHAp and CaFAp improves notably their performance. However, Pd(*z*)/CaHAp (Fig. 10) is much more active than Pd(*z*)/CaFAp (Fig. 11). The activity of the former increases with palladium loading and approaches 100% at 400 ˚C (Fig. 10). Conversely, the conversion on

Pd(*z*)/CaFAp (Fig. 11) increases very slowly with the temperature and reaches a maximum for Pd(0.5)/CaFAp. However, the conversion is around 30% at 450 °C and approches 100% only near 800 °C. Table 3 reports and compares the present results with those drawn from the literature. It also displays the temperatures at which the catalysts conversion reaches 10, 30, 50 and 90%.

The differences between of Pd(*z*)/CaHAp and Pd(*z*)/CaFAp probably result from the size of PdO particles and their inter- actions with the carrier. It is well established that PdO is decomposed to Pd at around 700 °C, provoking a drastic change in the catalyst activity [39].

(i) On Pd(*z*)/CaHAp the activity reaches 100% in the range 400–600 °C (depending on the Pd content) (Fig. 10), well below the announced decomposition temperature of PdO. According to UV–vis diffuse reflectance spectra of Pd(*z*)/CaHAp recorded after the catalytic run, PdO is par- tially reduced to Pd by the reaction mixture at 300 °C (Fig. 12b). Indeed, the massif centred near 450 nm and the absorption edge of PdO (located near 550 nm) suffers a marked decrease. Concomitantly, the background absorbance increases when λ decreases, attesting the presence of metal particles [40]. However, PdO is still detected in the sample up to 800 °C (Fig. 12c).

(ii) With Pd(*z*)/CaFAp the low activity observed and the appearance of a plateau for $z = 1$ and $z = 2$ (Fig. 11) might be due to the reduction PdO to Pd under reaction conditions. Indeed, PdO is still present after catalytic test at 300 °C but no more detected after test at 800 °C (Fig. 12e,f).

Hence, in Pd(1)/CaFAp, Pd remains in the reduced state after being exposed to reaction conditions (850 °C). Conversely, in Pd(1)/CaHAp, PdO is still present with Pd. Some authors have shown that the rate of oxidation of palladium itself is influenced by the particle size, the small particles showing a higher tendency to be oxidized [41,42]. Pd(1)/CaHAp is more efficient than Pd(1)/CaFAp in CH_4 oxidation. The metallic palladium resulting from the reduction is partially reoxidized by the oxy- gen of the reaction mixture, generating a more active PdO. Large discussions describing the activity of Pd and PdO are reported by the literature [39–45]. Recent results concerning Pd/alumina showed

that the small Pd particles (< 5 nm) are oxidized very rapidly whereas the oxidation of largest particles proceeds through a two steps fast and slow process [42]. There- fore, the Pd/CaHAp catalysts have a greater ability to undergo redox processes as in Mars and van Krevelen mechanism, the presence of Pd/PdO interfaces generating oxygen mobility. The importance of oxygen mobility has been reported, especially for $Pd/TiO_2/Al_2O_3$ catalysts [13]. In our case, this dynamic behaviour, generating surface redox cycles and surface defects seems to determine the activity. In the case of palladium, investigations have shown that the periodic changes of the surface increase the system dimensionality and might lead to oscillatory behaviour [45].

Finally, FTIR spectroscopy and XRD patterns of the samples after the catalytic runs did not show any significant difference with that of the original samples suggesting that the catalysts structure did not undergo any noticeable modification during the reaction.

4. Conclusion

Fluoration of hydroxyapatite has a marked effect on the properties of the support and on the catalytic behaviour of supported palladium. The PdO particles are smaller on Pd(*z*)/CaHAp than on Pd(*z*)/CaFAp. In butan-2-ol conver- sion, dehydrogenation (MEK production) predominates over dehydration (butenes formation) for both supports and cat- alysts. Moreover, significant differences appear: (i) below 180 °C, Pd(*z*)/CaHAp is more efficient in MEK production than Pd(*z*)/CaFAp; (ii) above 180 °C, Pd(*z*)/CaHAp is active in butanol combustion whereas Pd(*z*)/CaFAp is not, which may be related to differences in surface acidity and PdO particle size.

In methane combustion, the Pd(*z*)/CaHAp catalysts are much more active than Pd(*z*)/CaFAp. The presence of fluor seems to favour the reduction of PdO in the methane–air mixture and to prevent the reoxydation of palladium as required by the redox process.

Acknowledgments

The authors are indebted to the French “Ministère des affaires étrangères” for financial support (Action Integreée 183/MA/02) and to M. F. Herbst (ITODYS, University of Paris 7) for TEM examination.

References

[1] C.A. Muller, M. Maciejewski, R.A. Koeppel, A. Baiker, J. Catal. 166 (1989) 36.

[2] M. Lyubovsky, L. Pfefferle, A. Datye, J. Bravo, T. Nelson, J. Catal. 187 (1999) 275.

[3] D. Ciuparu, F. Bozon-Verduraz, L. Pfefferle, J. Phys. Chem. B 106 (2002) 3434.

[4] K. Eguchi, H. Arai, Appl. Catal. A: Gen. 222 (2001) 359.

[5] H. Widjaja, K. Seikizawa, K. Eguchi, H. Arai, Catal. Today 35 (1997) 197.

[6] R. Spinicci, A. Tofanari, Appl. Catal. A: Gen. 227 (2002) 159.

[7] T.V. Choudhary, S. Banerjee, V.S. Choudhary, Catal. Commun. 6 (2005) 97.

[8] M. Lyubovsky, L. Pfefferle, Catal. Today 47 (1999) 29.

[9] S.R.G. Carrazan, R. Mateos, V. Rives, P. Ruiz, Catal. Today 112 (2006) 161.

[10] V.V. Alegre, M.A.P. Silva, M. Schmal, Catal. Commun. 7 (2006) 314.

[11] K. Fujimoto, F.H. Ribeiro, M. Avalos-Borja, E. Iglesia, J. Catal. 179 (1998) 431.

[12] J.N. Carstens, S.C. Su, A.T. Bell, J. Catal. 176 (1998) 136.

[13] W. Lin, L. Lin, Y.X. Zhu, Y.C. Xie, K. Scheurell, E. Kemnitze, J. Mol. Catal. A: Chem. 226 (2005) 263.

[14] X. Zhang, C.S.-M. Lee, D.P. Mingos, D.O. Hayward, Appl. Catal. A 240 (2003) 183.

[15] Y. Deng, T.G. Nevell, J. Mol. Catal. 142 (1999) 51.

[16] G.W. Graham, D. Konig, B.D. Poindexter, J.T. Remillard, W.H. Weber, Top. Catal. 8 (1999) 35.

[17] C.A. Muller, M. Maciejewski, R.A. Koeppel, A. Baiker, J. Catal. 166 (1997) 36.

[18] L.M.T. Simplicio, S.T. Brandao, E.A. Sales, L. Lietti, F. Bozon-Verduraz, App. Catal. A

63 (2006) 9.

[19] K. Egushi, H. Arai, Appl. Catal. A 222 (2001) 359.

[20] T.R. Baldwin, R. Burch, Appl. Catal. 66 (1990) 359.

[21] F. Abbattista, A. Demastro, G. Gozzelina, D. Mazza, M. Vallino, G. Busca, V. Lorenzelli, J. Chem. Soc. Faraday Trans. 86 (1999) 3653.

[22] J.C. Elliot, Structure and Chemistry of the Apatites and other Calcium Orthophosphates, Elsevier, Amsterdam, 1994.

[23] K. El-Kabouss, M. Kacimi, M. Ziyad, S. Ammar, F. Bozon-Verduraz, J. Catal. 226 (2004) 16.

[24] M. Wakamura, K. Kandori, T. Ishikawa, Colloids Surf. A 142 (1998) 107.

[25] A. Crosman, G. Gelbard, G. Poncelet, V.I. Parvulescu, Appl. Catal. A 264 (2004) 23.

[26] J.A.S. Bett, W.K. Hall, J. Catal. 10 (1968) 105.

[27] C.L. Kibby, W.K. Hall, J. Catal. 29 (1973) 144.

[28] L. Bernard, M. Freche, J.L. Lacout, B. Biscans, Phosphorus Res. Bull. 10 (1999) 364.

[29] (a) K.C. Blakeslee, R.A. Condrate Sr., J. Am. Ceram. Soc. 54 (1971) 559;
(b) S.J. Joris, C.H. Amberg, J. Phys. Chem. 75 (1971) 3172.

[30] V.M. Bhatnagar, Bull. Soc. Chim. Fr. 8 (1968) 1771.

[31] Inorganic Crystal Structure Data Base (ICSD), National Institute of Stan- dards and Technology (NIST), release 2004/2.

[32] A. Rakai, D. Tessier, F. Bozon-Verduraz, New J. Chem. 16 (1992) 869.

[33] A. Rakai, A. Bensalem, J. C. Muller, D. Tessier, F. Bozon-Verduraz, Pro- ceedings of the 10th International Congress on Catalysis, 19–24 July, 1992, Budapest, Hungary, Guczi et al. (Ed.), New Frontiers in Catalysis, Elsevier Science Pub. (1993).

[34] (a) R.S. Weber, J. Catal. 151 (1995) 470;
(b) R.S. Weber and F. Bozon-Verduraz, Book of Abstracts, 212th ACS National

Meeting, Orlando, FL, August 25–29, 1996.

[35] (a) Y. Brik, M. Kacimi, F. Bozon-Verduraz, M. Ziyad, J. Catal. 202 (2001) 118;

(b) Y. Brik, M. Kacimi, F. Bozon-Verduraz, M. Ziyad, Microporous Meso- porous Mater. 43 (2001) 103.

[36] M. Moreno, A. Rosas, J. Alcaraz, M. Hernandez, S. Toppi, P. Da Costa, Appl. Catal. A 251 (2003) 369.

[37] J. El-Idrissi, M. Kacimi, F. Bozon-Verduraz, M. Ziyad, Catal. Lett. 56 (1998) 221.

[38] Y. Matsumura, H. Kanai, J.B. Moffat, J. Mol. Catal. A 115 (1997) L229.

[39] R.J. Farrauto, M.C. Hobson, T. Kennelly, E.M. Waterman, Appl. Catal. A 81 (1992) 227.

[40] (a) J.G. McCarty, Catal. Today 26 (1995) 283;

(b) P.O. Thevenin, A. Alcade, L.J. Pettersson, S.G. Ja¨ras, J.L.G. Fierro, J. Catal. 215 (2003) 78.

[41] R.F. Hicks, H. Qi, M.L. Young, R.G. Lee, J. Catal. 122 (1990) 280.

[42] D. Roth, P. Gelin, A. Kaddouri, E. Garbowski, M. Primet, E. Tena, Catal. Today 112 (2006) 134.

[43] R.F. Hicks, H. Qi, M.L. Young, R.G. Lee, J. Catal. 122 (1990) 295.

[44] E. Garbowski, C. Feumi-Jantou, N. Mouaddib, M. Primet, Appl. Catal. A 109 (1994) 277.

[45] L.M.T. Simplicio, S.T. Brandao, E.A. Sales, L. Lietti, F. Bozon-Verduraz, Appl. Catal. B 63 (2005) 9.

Catalysts	Chemical analyses (wt%)			S (m^2/g)
	Pd	Ca	P	
CaHAp	0	38.65	18.99	69.2
Pd(0.3)/CaHAp	0.29	–	–	62.3
Pd(0.5)/CaHAp	0.51	–	–	67.5
Pd(1)/CaHAp	1.01	–	–	67.6
Pd(2)/CaHAp	2.09	36.39	18.95	66
CaFAp	0	37.09	18.15	48
Pd(0.3)/CaFAp	0.31	–	–	46.8
Pd(0.5)/CaFAp	0.52	–	–	47.4
Pd(1)/CaFAp	1.03	–	–	49.6
Pd(2)/CaFAp	2.06	35.47	18	49.6

Table 1. Specific surface areas of the catalysts calcined at 550 ˚C

Wavelength (λ, nm)	Catalysts or reference compound	Transition mode	Reference
380	$Pd(acac)_2$	d–d ($\nu_1 + \nu_2$)	[25]
625	$PdCl_4^{2-}/Al_2O_3$	d–d (ν_1') spin forbiden	
475		d–d ($\nu_1 + \nu_2$)	
335		d–d (ν_3)	
280		(ν_4): metal-ligand, C.T.[a]	
450	PdO/Al_2O_3 ex $(PdCl_2)$[b]	d–d ($\nu_1 + \nu_2$)	
380	PdO/Al_2O_3 ex $Pd(NO_3)_2)$[b]	d–d ($\nu_1 + \nu_2$)	
460	Pd/NaY	d–d ($\nu_1 + \nu_2$)	
460	PdO/Al_2O_3 ex $(Pd(acac)_2)$[b]	d–d ($\nu_1 + \nu_2$)	
250	Pd(z)/CaHAp	Pd–O: C.T.[a]	This work
375		d–d ($\nu_1 + \nu_2$)	
475		d–d (ν_3)	
250; 275	Pd(z)/CaFAp	Pd–O and Pd–F: (C.T.)[a]	This work
375		d–d ($\nu_1 + \nu_2$)	
475		d–d (ν_3)	

[a] C.T., charge transfer.
[b] Pd compound used for the impregnation.

Table 2. Position and attribution of UV–vis bands of the catalysts and reference compounds

Catalysts	S (m^2/g)	T_{10}(°C)	T_{30}(°C)	T_{50}(°C)	T_{90}(°C)	References
CaHAp	69.2	635	720	785	865	This work
$Pd_{0.3}$CaHAp	62.3	345	400	450	560	
$Pd_{0.5}$CaHAp	67.5	360	415	460	575	
Pd_1CaHAp	67.6	330	380	415	500	
Pd_2CaHAp	66	325	375	410	500	
CaFAp	48	725	750	765	800	
$Pd_{0.3}$CaFAp	46.8	560	625	700	825	
$Pd_{0.5}$CaFAp	47.4	370	445	535	800	
Pd_1CaFAp	49.6	430	700	810	870	
Pd_2CaFAp	49.6	725	780	845	875	
$Pd_{1.1}SnO_2$	6.4	325	355	–	490	[4]
$Pd_{1.1}Al_2O_3$	110.1	340	370	–	500	[5]
$Pd_{1.1}NiO$	2.6	390	480	–	590	[5]
$Pd_{1.1}Al_2O_3$–36NiO	13.6	320	340	–	470	[5]
Pd_1–ZrO_2	5.6	325	355	–	490	[16]

Table 3. Catalytic activity of Pd(z)/CaHAp et Pd(z)/CaFAp in CH4 oxidation and comparison with some literature data

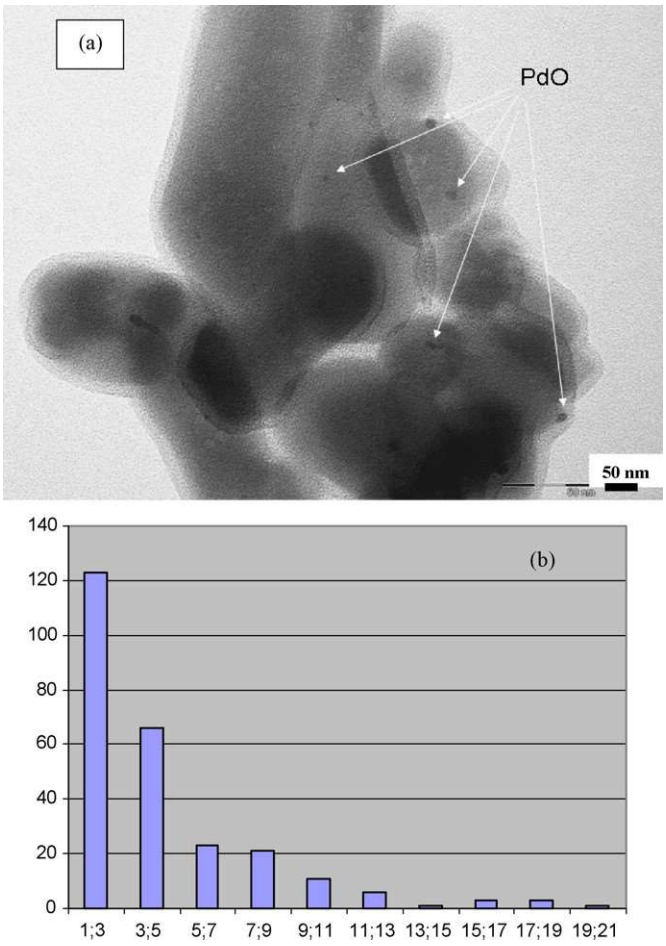

Fig. 1. TEM image (a) and size distribution (b) of Pd(1)/CaHAp.

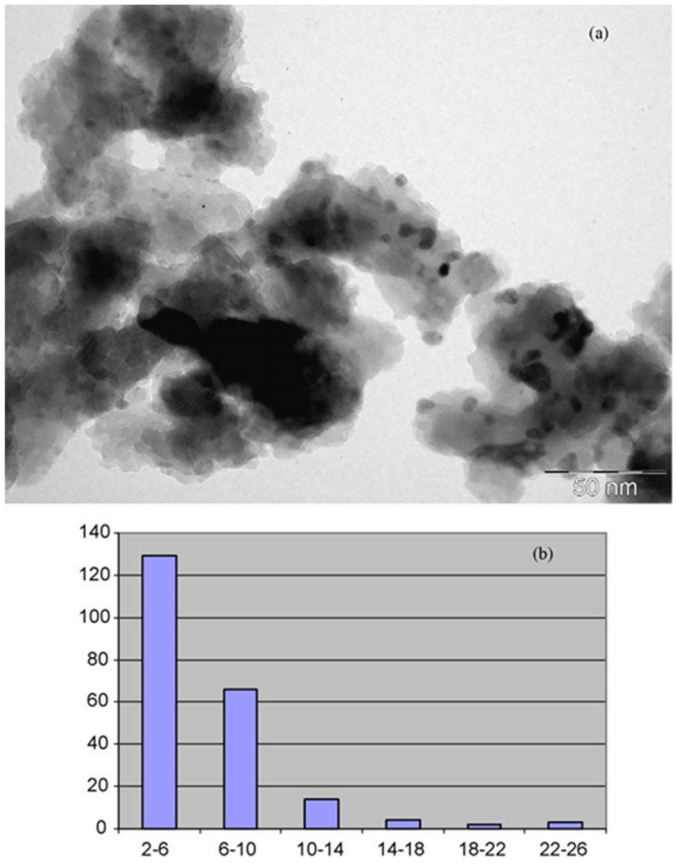

Fig. 2. TEM image (a) and size distribution (b) of Pd(1)/CaFAp

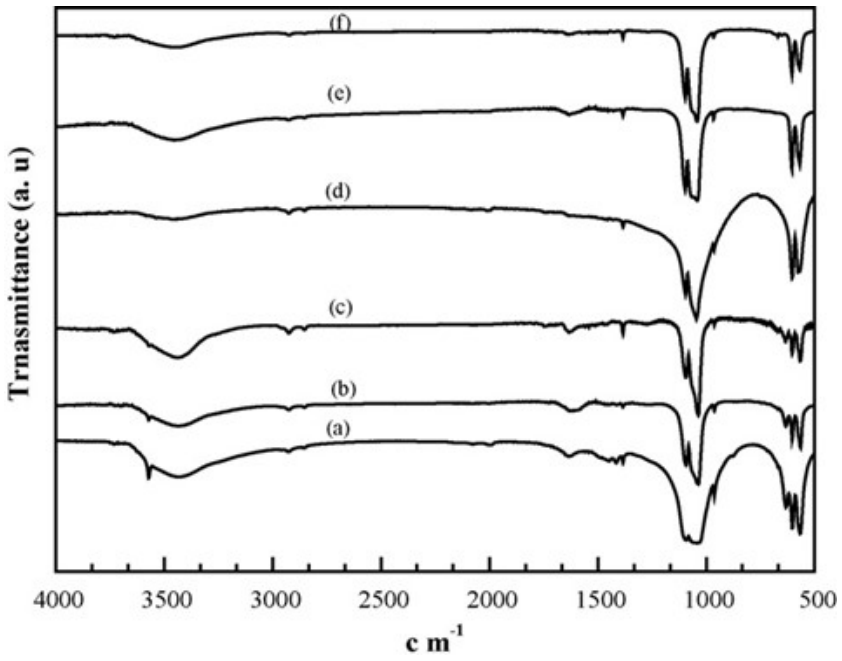

Fig. 3. FTIR spectra of Pd(*x*)/CaHAp and Pd(*x*)/CaFAp calcined at 550 ˚C. (a) CaHAp; (b) Pd(1)/CaHAp; (c) Pd(2)/CaHAp; (d) CaFAp; (e) Pd(1)/CaFAp; (f) Pd(2)/CaFAp.

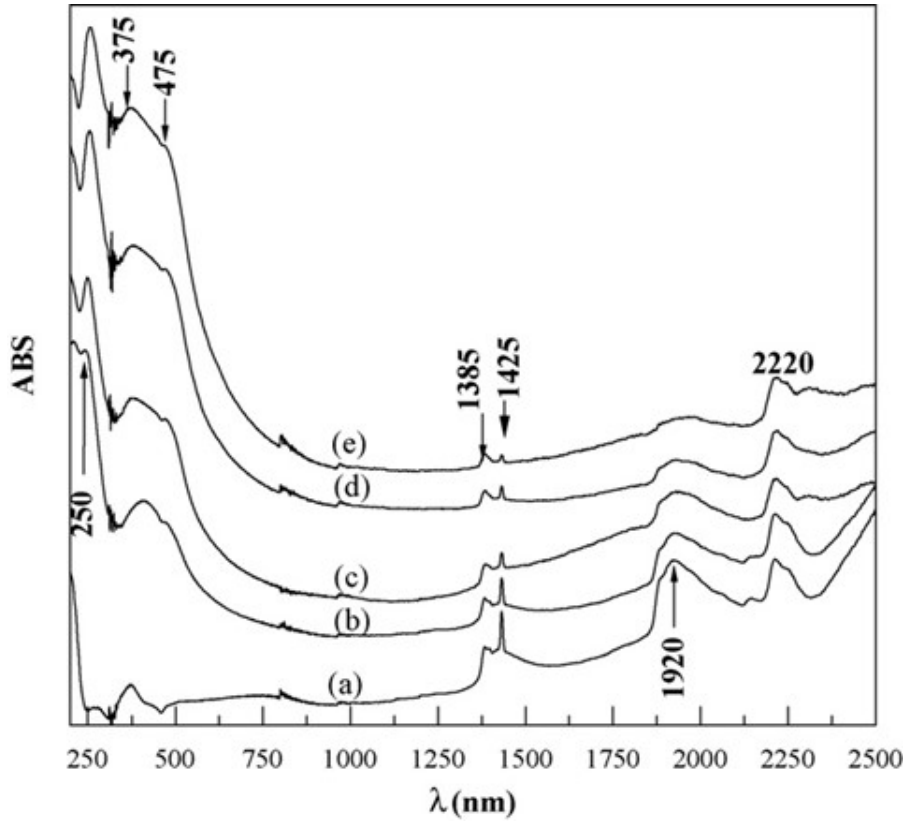

Fig. 4. UV–vis–NIR spectra of Pd(z)/CaHAp loaded with (a) $z = 0\%$; (b) $z = 0.3\%$; (c) $z = 0.5\%$; (d) $z = 1\%$; (e) $z = 2\%$; calcined at 550 °C under air.

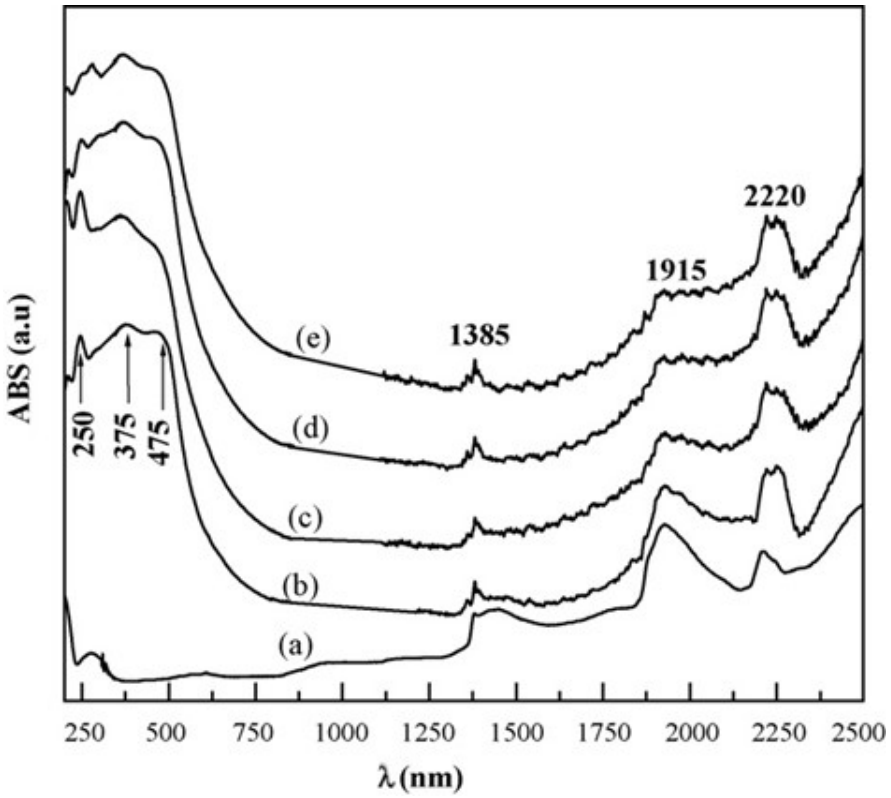

Fig. 5. UV–vis–NIR spectra of Pd(z)/CaFAp loaded with (a) $z = 0\%$; $z = 0.3\%$; (c) $z = 0.5\%$; (d) $z = 1\%$; (e) $z = 2\%$; calcined at 550 °C, under air.

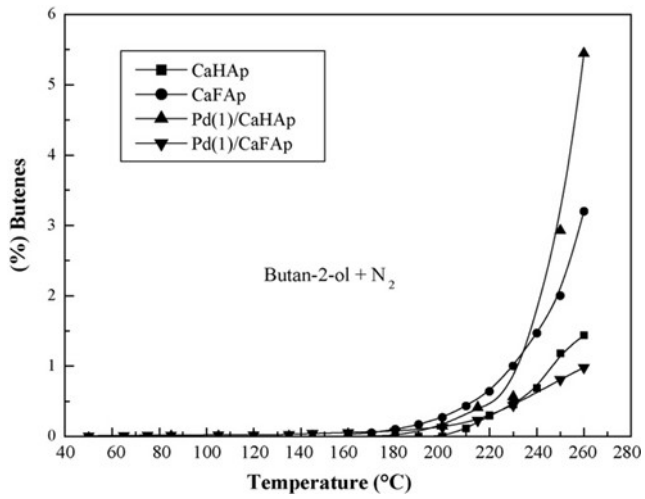

Fig. 6. Butan-2-ol conversion into butenes, in the absence of O_2, over CaHAP, CaFAp, Pd(1)/CaHAp and Pd(1)/CaFAp.

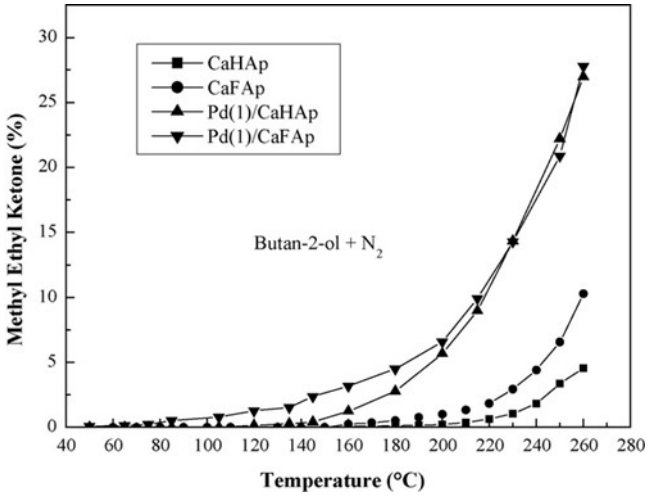

Fig. 7. Butan-2-ol conversion into methyl ethyl ketone, in absence of O_2, over CaHAp, CaFAp, Pd(1)/CaHAp and Pd(1)/CaFAp

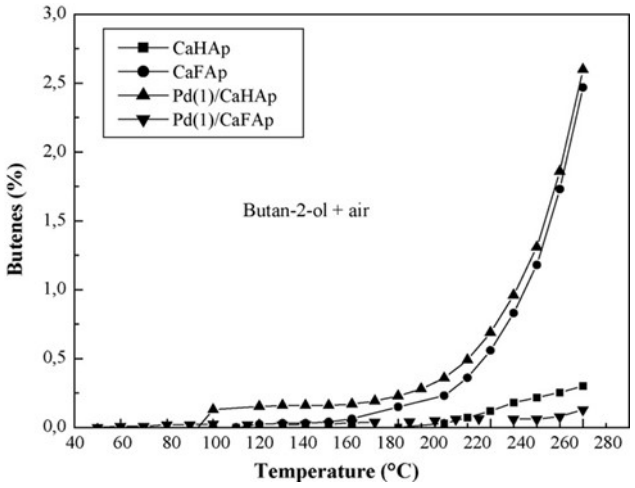

Fig. 8. Butan-2-ol conversion into butenes, in presence of O_2, over CaHAp, CaFAp, Pd(1)/CaHAp and Pd(1)/CaFAp.

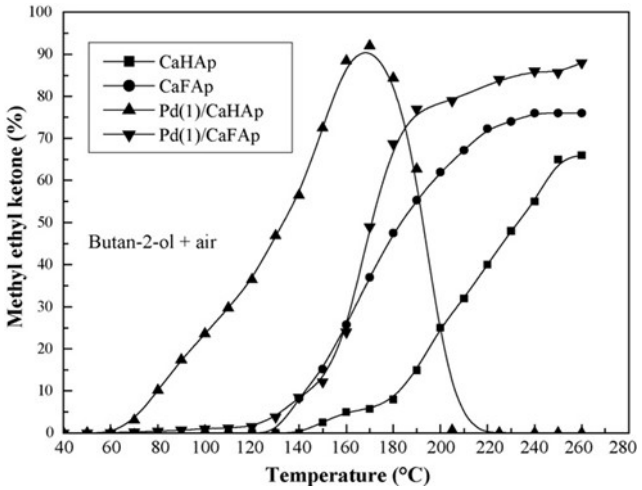

Fig. 9. Butan-2-ol conversion into methyl ethyl ketone, in presence of O_2, over CaHAp, CaFAp, Pd(1)/CaHAp and Pd(1)/CaFAp.

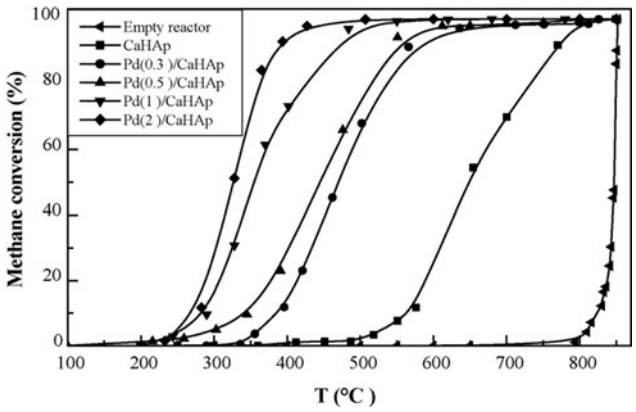

Fig. 10. Methane oxidation over Pd(z)/CaHAp vs. the reaction temperature. (The composition of the reaction mixture being: 1% CH_4, 99% Air).

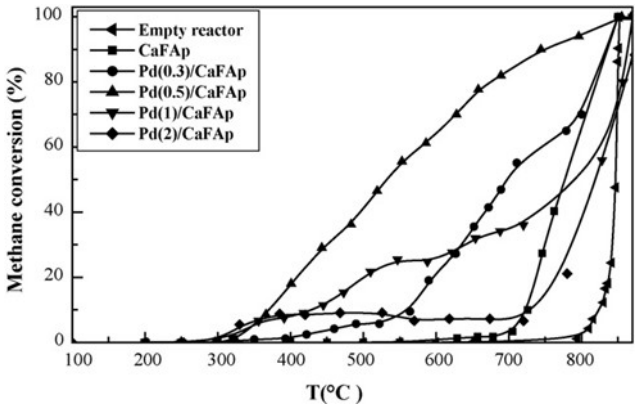

Fig. 11. Methane conversion over Pd(*z*)/CaFAp vs. the reaction temperature. (The composition of the feeding stream being: 1 vol% CH_4, 99 vol% air).

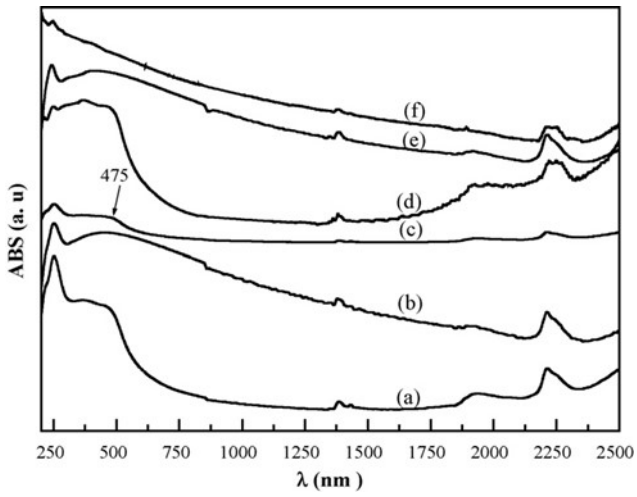

Fig. 12. Comparison of UV–vis–NIR of (a) Pd(1)/CaHAp; (b) Pd(1)/CaHAp after the test at 300 ˚C; (c) Pd(1)/CaHAp after test at 800 ˚C; (d) Pd(1)/CaFAp; (e) Pd(1)/CaFAp after test at 300 ˚C; (f) Pd(1)/CaFAp after test at 800 ˚C.